International Journal of Fatigue 31 (2009) 385–392

Contents lists available at ScienceDirect

International Journal of Fatigue

journal homepage: www.elsevier.com/locate/ijfatigue

Thermoelasticity and CCD analysis of crack propagation in AA6082 friction stir welded joints

P. Cavaliere [a,*], A. De Santis [a], F. Panella [a], A. Squillace [b]

[a] Department of Innovation Engineering, Engineering Faculty, University of Salento, I-73100-Lecce, Italy
[b] Department of Materials and Production Engineering, University of Naples "Federico II", I-80125 Naples, Italy

ARTICLE INFO

Article history:
Received 25 February 2008
Received in revised form 10 June 2008
Accepted 24 July 2008
Available online 19 September 2008

Keywords:
Friction stir welding
Crack propagation
Thermoelasticity
CCD
Fatigue

ABSTRACT

The advantages of friction stir welding (FSW) process compared to conventional fusion welding technologies have been clearly demonstrated in recent years. In the present study, AA6082 FSW joints were produced by employing different welding parameters. The principal aim of this work is to apply thermoelastic stress analysis (TSA) to study crack propagation characteristics of friction stir welded aluminum sheets, during cyclic fatigue tests. The crack propagation experiments were performed by employing single edge notched specimens; fatigue tests were performed under tension with load ratio $R = 0.1$. All the mechanical tests were conducted up to failure. The TSA measurement system allowed crack evolution to be observed in real-time during fatigue cycles and stress fields to be derived on the specimens from the measured temperature variation. The thermoelastic data were used to analyse principal stresses and principal strains on the specimens surface and the crack growth rate during tests. In addition, it was possible to evaluate all the joints defects effects, as a function of welding parameters, correlating effects on different crack growth rate and instabilities. The achieved results were compared with those obtained by classical CCD camera monitoring of crack front propagation during cyclic loading and all the results were validated by employing finite element analysis performed with ABAQUS software.

1. Introduction

Friction stir welding technology has been demonstrate to produce very good and sound joints especially in the applications for light alloys [1]. Based on friction heating at the faying surfaces of two sheets to be joined, in the FSW process a tool with a specially designed rotating probe travels down the length of contacting metal plates, producing an highly plastically deformed zone through the associated stirring action. The localized thermo-mechanical affected zone is produced by friction between the tool shoulder and the plate top surface, as well as plastic deformation of the material in contact with the tool occurs [2]. The probe is typically slightly shorter than the thickness of the work piece and its diameter is typically slight larger [3]. The microstructure evolution and the resulting mechanical properties depend strongly on the processing parameters variation, leading to a wide range of possible performances in use [1,4]; in particular it was observed that the optimal mechanical properties are obtained in those joints welded with an advancing/rotating speed rate in the range 0.1–0.2 mm/revolution (revolutionary pitch). Many interesting papers have been published on the fatigue properties of FSW aluminium alloys, showing the far higher properties with respect to the conventional fusion welding techniques [5–9]. In addition, such technique allows to weld dissimilar alloys and materials obtaining very high joints strength [10].

It can be observed in particular that the fatigue strength of the FSW weld decreases with increasing tool travel speed/rotation rate ratio due to the increase of non-welded groove on the root side of the weld [11]. It was also observed that when a clockwise direction rotation is employed, the less resistant area is found to be the one on the advancing tool side.

2. Experimental procedure

2.1. Materials and methods

The material under investigation was a 6082 commercial aluminium alloy produced by Pechiney under the form of rolled plates of 4 mm thickness. Large plates 200 mm length × 80 mm width, were welded perpendicularly to the rolling direction, after standard T6 heat treatment. Such thermal treatment offers a considerable improvement of the material corrosion resistance. Six different welding conditions were studied; the employed rotating speeds and advancing speeds of the threaded tool were 1600 RPM rotation with 230, 325, 460 mm/min speeds and 1000 RPM rotation with 165, 230 and 325 mm/min, respectively. The nib of the tool had a diameter of 6.0 mm and was 3.9 mm long. A 14 mm diameter

* Corresponding author. Tel.: +39 0832297324; fax: +39 0832325004.
E-mail address: pasquale.cavaliere@unile.it (P. Cavaliere).

0142-1123/$ - see front matter © 2008 Elsevier Ltd. All rights reserved.
doi:10.1016/j.ijfatigue.2008.07.016

shoulder was used and the tilt angle was set equal to 3°, according to previous welding experiments. All the specimens surfaces were machined in order to eliminate all the surface asperities. The residual stresses beside the weld line were calculated in longitudinal direction with respect to the load by employing the $\sin^2\Psi$ method [12]. The residual stresses were measured in longitudinal direction with respect to specimen one, being the notch perpendicular to the loading direction and consequently being the ones affecting the crack tip stress field. Tensile tests were performed in order to evaluate the mechanical properties of the joints obtained in the different welding conditions. The load is applied transversally to the weld cord; the tensile tests were done at room temperature using a MTS 810 testing machine with initial strain rate of 10^{-3} s^{-1}. Specimens were sectioned perpendicularly to the weld line by employing an electrical discharge machine (EDM). The fatigue crack experiments were performed by a resonant electro-mechanical testing machine under constant loading control up to 100 Hz, with sine wave loading (TESTRONIC^{TM} 50 ± 25 kN, produced by RUMUL, SUI) and by employing single edge notched specimens (1 mm depth) obtained at 6 mm from the weld center on the advancing side. For all the tested materials a value of $R = 0.1$ was used.

2.2. Principles of applied TSA

Experiments aimed at determining endurance limit and critical crack factors are generally costly and time consuming, either for laboratory samples or complicated industrial components. For this reason, non-destructive evaluation (NDE) techniques are playing an increasing role in the structural integrity evaluation and failure prevention. There exist many non-destructive techniques, available to monitor mechanical damage including X-ray, acoustic emission and ultrasonic methods. However, these methods present their own different limitations. In most cases they operate locally and/or require special sample preparation and experienced operator skills. Not many papers exist instead about the fatigue behavior evaluation using thermographic infrared techniques [13–16]. Crack propagation has been more and more studied in the last two decades using the SPATE (stress pattern analysis by thermal emission) system [17], which allowed the determination of fatigue stress field, based on the evaluation of the thermoelastic effect. Advanced IR cameras called differential cameras have been developed to analyze the local varying temperature component and therefore the thermoelastic effect rather than the overall temperature field (due also to the inelastic effect and the heat conduction effect), as in classical thermographic measurements. The more recently developed DeltaTherm system makes it possible to actually perform real-time crack propagation investigation based on a much faster data collection [18]. This opens up the possibility of identifying in real-time, i.e. while the test is actually being performed, the presence of crack initiations and propagation [19]. By accurately determining the calibration factor, which relates the measured temperature oscillation to the stress variation, it also becomes possible to analyze the stress field in the area where the crack initiated and during its evolution. According to authors knowledge, apart from a paper devoted to the thermoelastic study of welded ferritic steel plates [19], not much work may be found in the literature on the use of thermoelasticity techniques for the fatigue analysis of welded specimens. The samples were single-etched notched [19]

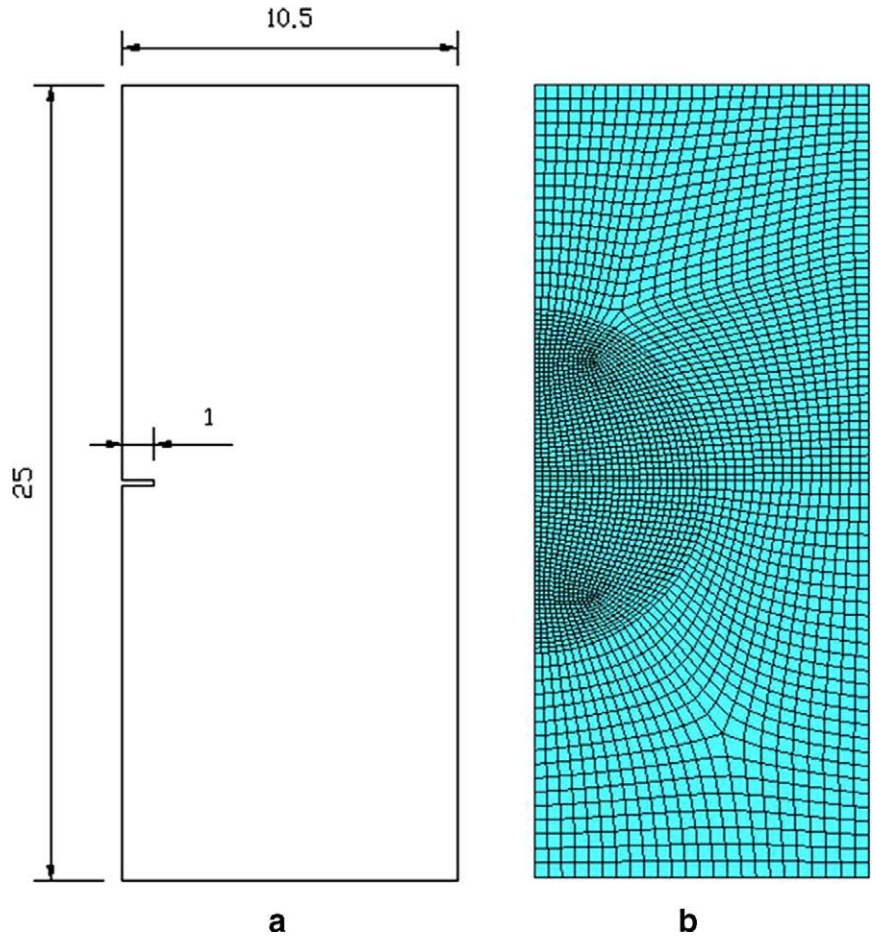

Fig. 1. Specimen geometry and the finite element mesh for small scale yielding problem solving for the single edge notch, all the units are in mm.

and the technique proved to be sensitive to the presence of residual stresses due to welding. In particular, the numerical stress intensity factor was evaluated taking into account the residual stresses effect (which was calculated using a weight function term) and subsequently compared to TSA experimental value. In the present case, the FSW technique does not present high residual stresses compared to traditional welding techniques; the use of TSA is therefore aimed at tracking the crack initiation and growth in relation to different areas in which it could take place; areas which are affected in various ways by the welding process.

The detailed description of the employed system and the application to different analysis are available in the literature [20–25].

2.3. Numerical evaluation

Unstable Crack propagation occurs when fracture parameters reach a critical value; the effective J-integral evaluation is largely recognized as an important method in the fracture mechanics problems. It is related to the energy release with the crack growth and gives the deformation measure at the crack tip [26].

For Mode I load, the characteristic stress intensity factor can be calculated by:

$$K_I = \left(\frac{EG}{1-(\alpha\upsilon)^2}\right)^{\frac{1}{2}} \quad (1)$$

The evaluation of the characteristic fracture parameters for the studied joints was performed by employing finite element simulations with ABAQUS software.

The mesh used for the simulations was built up using 4-nodes elements and the crack propagation zone simulation was performed with 1558 elements. The specimen geometry and the finite element mesh for small scale yielding problem is shown in Fig. 1.

The materials behavior was considered to be governed by the rate-independent plasticity theory with isotropic hardening. Loads were applied in incremental way, and the solution to the non linear boundary value problem at each increment was obtained by a fully implicit update using the Newton–Raphson method.

3. Results and discussion

The tensile strength of 6082 FSW joints obtained by tests is shown in Table 1. It can be observed how the maximum yield strength is reached with a rotating/advancing speed ratio between 6 and 7 for both the tool rotating speeds employed in the present study.

The fatigue endurance (S–N) curves of 3 of the studied joints are shown in Fig. 2. The joints welded with a rotation speed of the tool of 1600 RPM and a travel speed of 230 mm/min produce the highest fatigue resistance; the samples welded at 1600 RPM 325 mm/min and 1000 RPM 165 mm/min show very similar behaviour at high stress amplitude, but such difference decreases as the maximum applied stress. The remaining joints had a fatigue behaviour governed by the presence of big voids or tunnels which produced quick failures after few loading cycles, an example of such kind of defects is shown in Fig. 3.

The longitudinal profile of the residual stresses for the studied joints is shown in Fig. 4; it can be observed how the welds obtained with 1600 RPM and 230 mm/min or with 1000 RPM and 165 mm/min are characterised with residual stresses in the zone where the notch was obtained, which are in compressive state, while for the welds obtained at 1600 RPM and 325 mm/min they are in tensile conditions. In addition the compressive state is more pronounced for the joints welded at 1600 RPM.

The tool advancing action (inclined at a certain angle) is extremely similar to an extrusion process which requires optimal temperature conditions for the better quality of the material in terms of microstructure; consequently, since the resultant fatigue behavior for butt welded joints is directly related to the microstructure, provided that porosities occurrence is avoided and micro-cracks formation is absent, and considering that stress concentrators are missing, the studied FS Welded joints offer the best fatigue

Table 1
Yield strength of the studied joints as a function of the different welding parameters

Welding parameters	Yield strength (MPa)
1600 RPM, 230 mm/min	230
1600 RPM, 325 mm/min	180
1600 RPM, 460 mm/min	110
1000 RPM, 165 mm/min	150
1000 RPM, 230 mm/min	130
1000 RPM, 325 mm/min	80

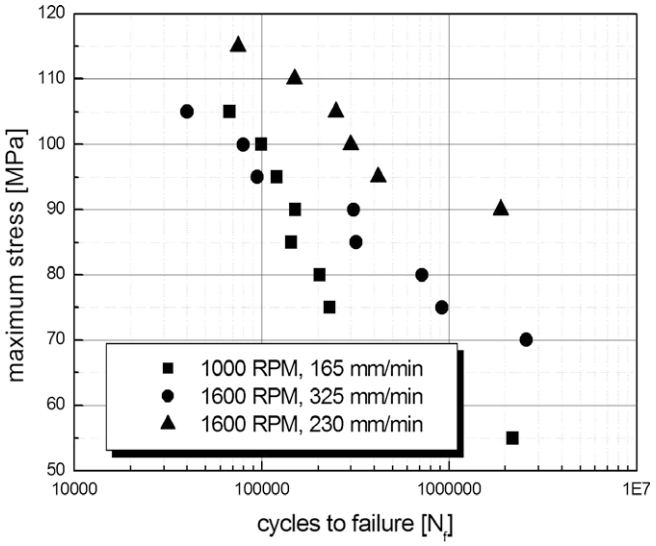

Fig. 2. Fatigue endurance curves for the joints welded with a rotation speed of the tool of 1600 RPM and travel speeds of 230 and 325 mm/min and 1000 RPM 165 mm/min.

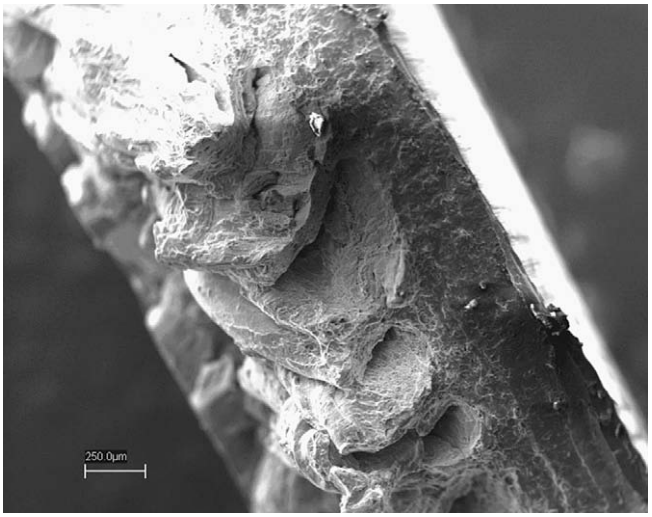

Fig. 3. Fracture surface of the joint welded at 1000 RPM 230 mm/min.

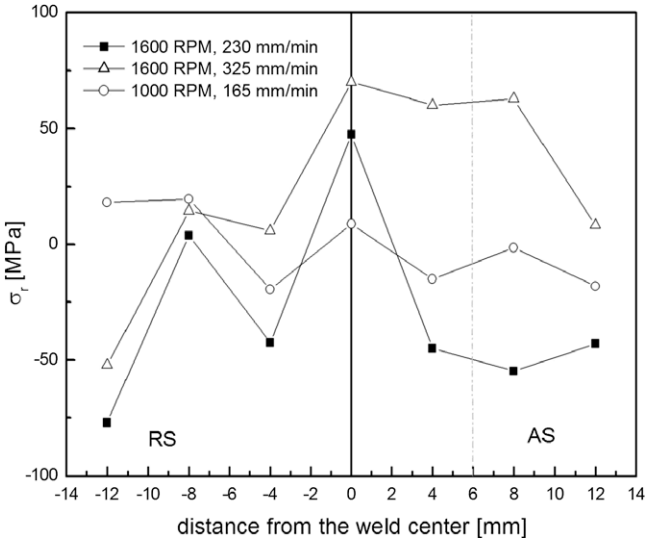

Fig. 4. Residual stress profile in longitudinal direction respect to the welding one for the fatigue tested joints.

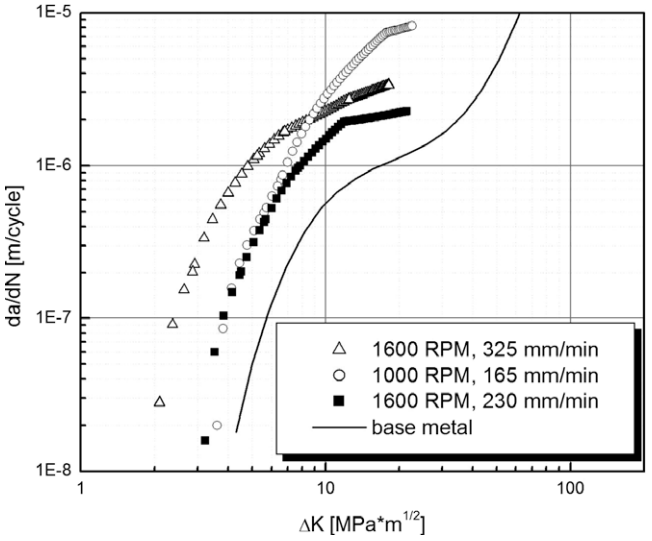

Fig. 5. The fatigue crack rate as a function of ΔK for all the joints at a load ratio of $R = 0.1$.

performances only when optimal microstructure configurations are reached. With a revolutionary pitch in the range of 0.07–0.1, the process is in the optimal temperature and strain rates conditions to produce good microstructure quality without defects for butt joints and therefore sound welds are achieved. The longitudinal residual stresses were measured in the cross sections of the welds by X-ray diffraction using the $\sin^2\Psi$ method. It must be observed that the residual stresses can be relaxed for the cut of the mechanical testing specimens, for this reason the residual stresses showed in the present work are related to the measurements performed on the cut material. As a general behavior, the residual stresses have compressive character by approaching the weld line, changing to a tensile character in the weld zone from the heat affected one. It can be observed that the higher values of residual stresses are achieved in the advancing side of the tool. The residual stresses values differences depend on the asymmetry of the FSW process; it is demonstrated by several finite element calculations that the higher deformation across the weld line are achieved in the retreating side of the tool when a clockwise direction is employed for the rotation. Such an higher deformation produces an

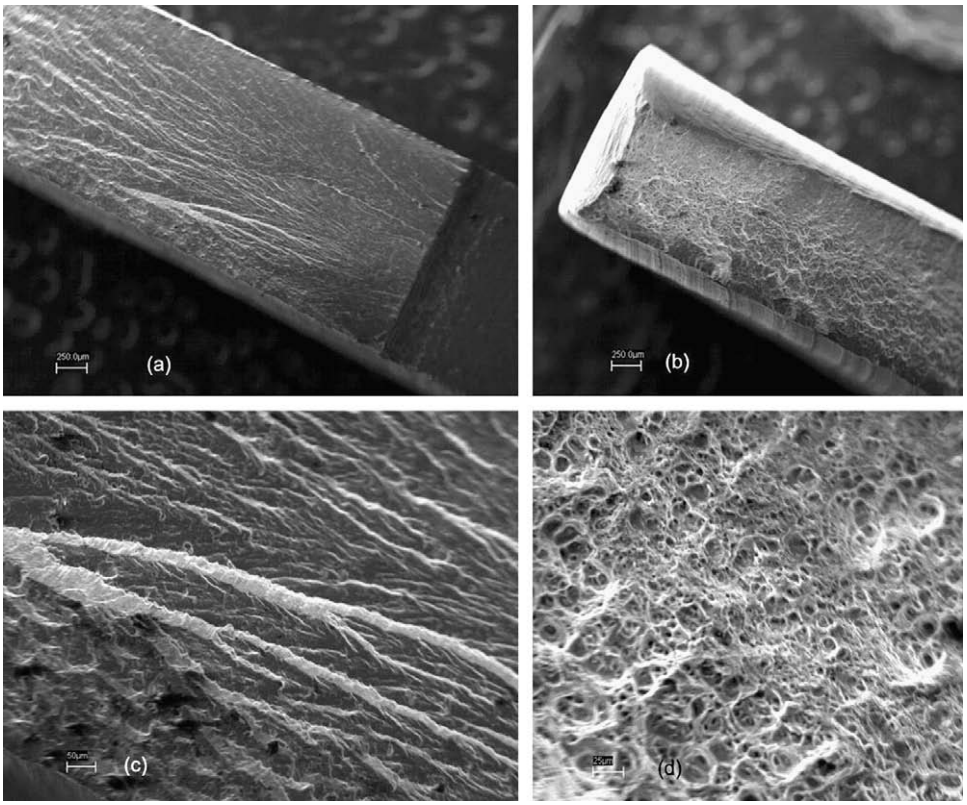

Fig. 6. Fracture surface of the specimen welded at 1600 RPM, 230 mm/min.

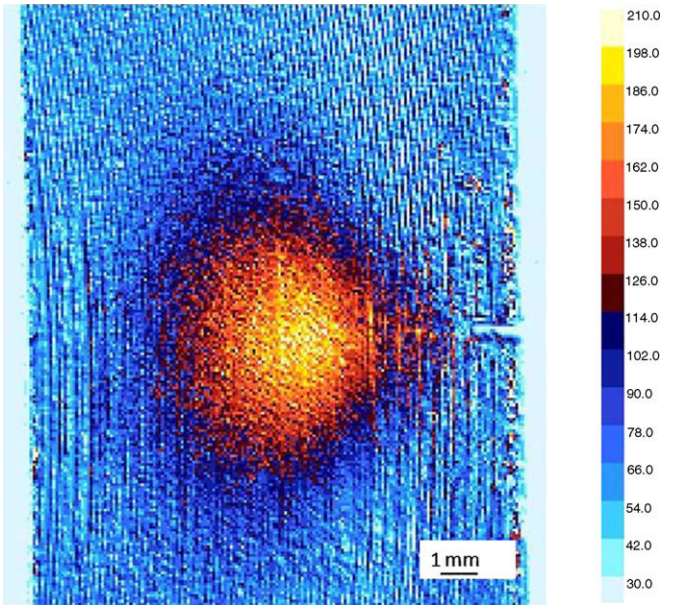

Fig. 7. Thermoelastic image representing the stress field map for the specimen welded at 1600 RPM, 230 mm/min after 31,400 cycles.

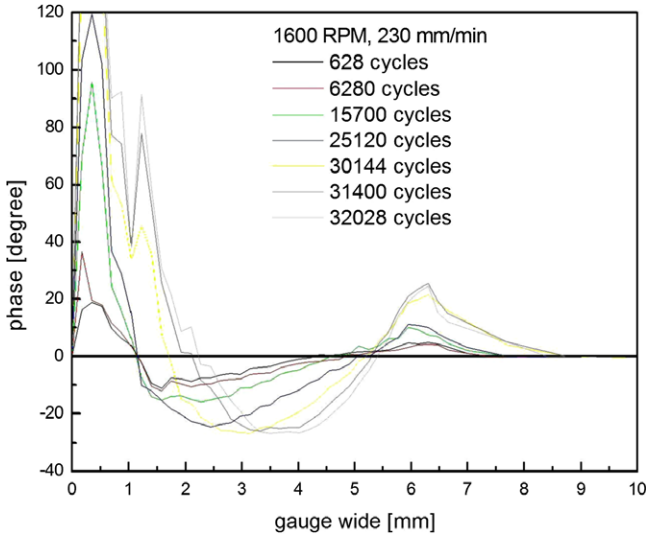

Fig. 9. Typical phase maps obtained by TSA measurements.

increase in the temperature respect to the advancing side leading to a softening during the process.

The fatigue crack rate as a function of ΔK for all the joints at a load ratio $R = 0.1$ is shown in Fig. 5. For all the tested specimens, the cracks propagate in direction perpendicular to the loading axis; it can be observed that the joints welded with a rotating speed of 1000 RPM are more sensitive to crack initiation with respect to the ones obtained at 1600 RPM. More over, the joints welded at 1600 RPM show a crack growth rate lower than those welded with a rotating speed of 1000 RPM. As a general behaviour, all the welds show a decrease in ΔK threshold and an increase in crack propagation rate with respect to the parent material. The residual stress state plays an important role in fatigue threshold value and cracks growth. The difference in ΔK threshold can be attributed to the longitudinal residual stress profile, in fact the welds in which a compressive state was measured show the resistance to crack initiation is higher. In addition, a different mechanism of crack closure acts during the cyclic loading as a function of the different residual stress state and is claimed to be responsible for the increased crack growth rate as decreasing the compressive residual stresses.

The cracks propagating in compressive fields grow slower with respect to the ones propagating in tension stress fields.

The fracture surface images of the sample welded at 1600 RPM, 230 mm/min are shown in Fig. 6; the material fractures principally by cleavage with local ductility features experienced especially in the final part of the fatigue life.

All the fatigue crack tests were monitored via thermoelastic stress analysis (TSA), providing the fullfield stress maps for the specimens surface, while subjected to cyclic loading. In order to achieve an higher resolution in the stress spatial distribution, the investigating area was restricted using suitable optics around the region where crack initiation was observed during preliminary tests (Fig. 6, specimen welded at 1600 RPM and 230 mm/min after 31,400 cycles). The crack initiation was observed in all the test loading conditions by means of thermal images. As already mentioned, when the material is loaded at high frequency in the elastic region, the thermoelastic data related to conduction are linearly proportional to the sum of principal stresses displayed in 2-D maps on the specimen surface at different crack growth stages and are shown in Fig. 7: crack formation and propagation is followed in

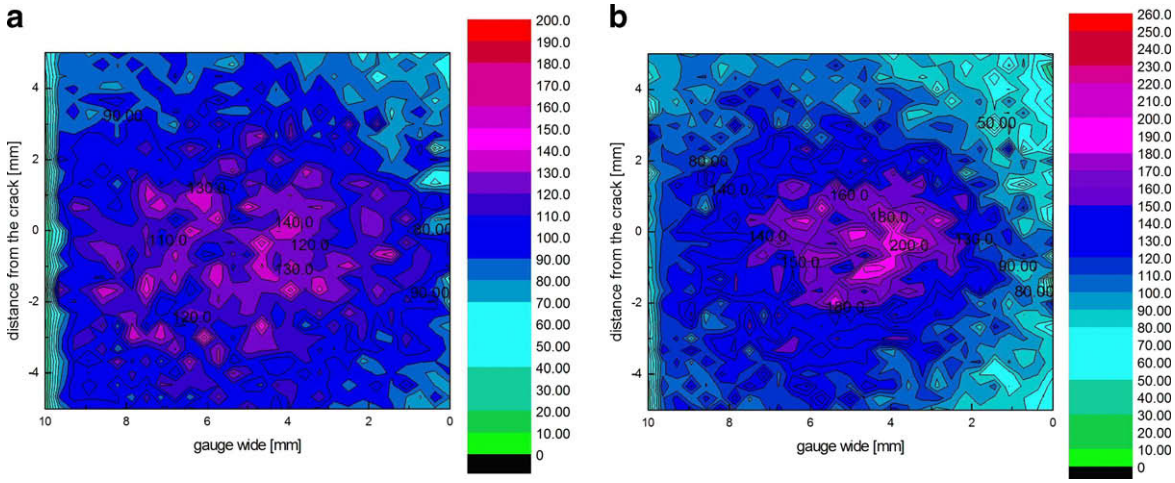

Fig. 8. Stress field maps for the specimen welded at 1600 RPM, 230 mm/min after 6280 (a) and 31,400 cycles.

real-time providing continuously the real stress fields around the crack tip, including closure effects.

All the stress maps were obtained using a scale factor K together with the output signal V from the measurement system [21]. Adiabatic conditions require also to verify that these are fulfilled, examining carefully the thermal images around the crack initiation area. In the surroundings of this zone, adiabatic conditions may fail to verify because of two basic phenomena and hence a change in phase: heat generation due to plastic work and the presence of high stress gradients, both occurring near the crack tip area. The effect of these phenomena on the thermoelastic images is a blurring effect around the crack tip area, which makes it difficult to determine visually the crack tip position. The exact location of the crack tip is important when, for example, the stress intensity factor is inferred from thermoelastic measured data; the loss of adiabaticity can be identified from the phase maps and from the examination of the different phase profiles (Fig. 8), since adiabatic conditions are achieved when the phase is constant and equal to zero. Observing the phase profile in Fig. 9, three different zones can be identified approaching the crack tip area [19]: (I) a region where the phase is constant and therefore adiabatic conditions are achieved; (II) a region where the phase starts assuming positive values indicating a loss of adiabaticity due to plasticity and high stress gradients; (III) a region where the phase is negative until the crack tip is reached, due probably to reverse plasticity effects. From the crack tip onwards the phase sign changes continuously, this fact being attributed probably to contact state between the crack faces and background reflections coming from inside the crack. In this way it is possible to calculate the end position of region III during the fatigue tests, relating it to the number of cycles. These data are used to infer the crack length and rate.

The change in the stress fields curves shape is therefore due to lack of adiabatic conditions and then to different heat generation and conduction due to the plastic deformation in the crack zone subjected to various cyclic loadings.

The principal stresses distribution directly measured and normalized around the crack site for different number of loading cycles is shown in Fig. 10. As expected, an increase of the stress values around the crack site was observed as increasing the number of cycles; the broadening of stress profiles around the crack by

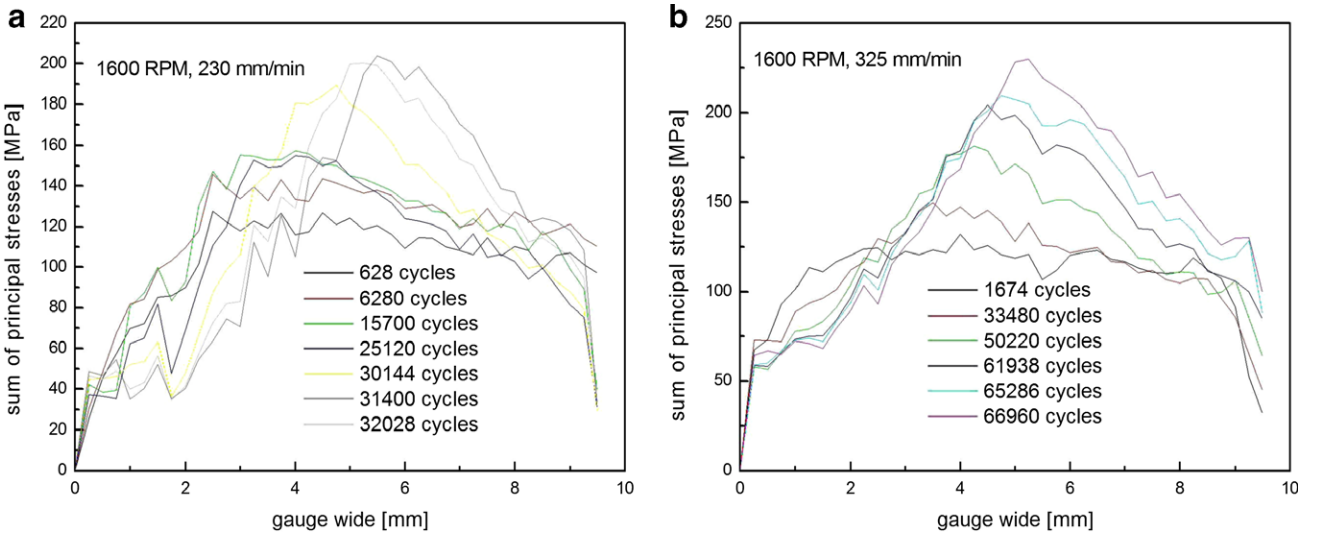

Fig. 10. Principal stresses distribution around the crack site at different stages of crack growth for two different welds tested during the present work.

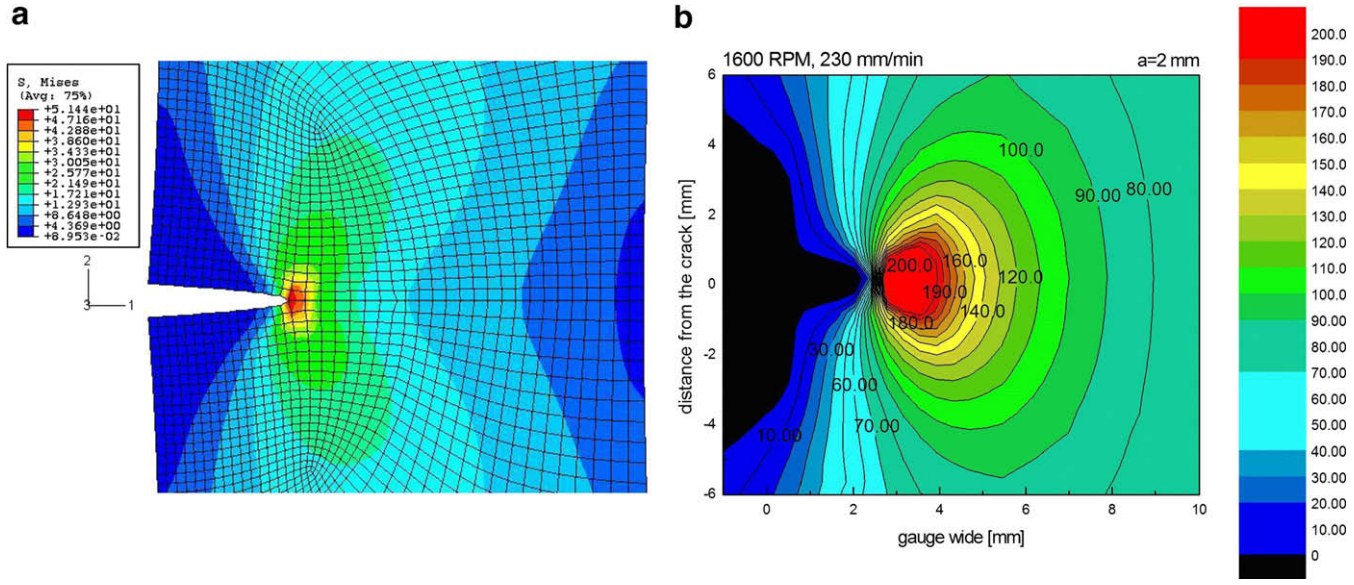

Fig. 11. Von Mises stress distribution (a) and stress field map for a crack length of 2 mm (b) obtained from ABAQUS calculations.

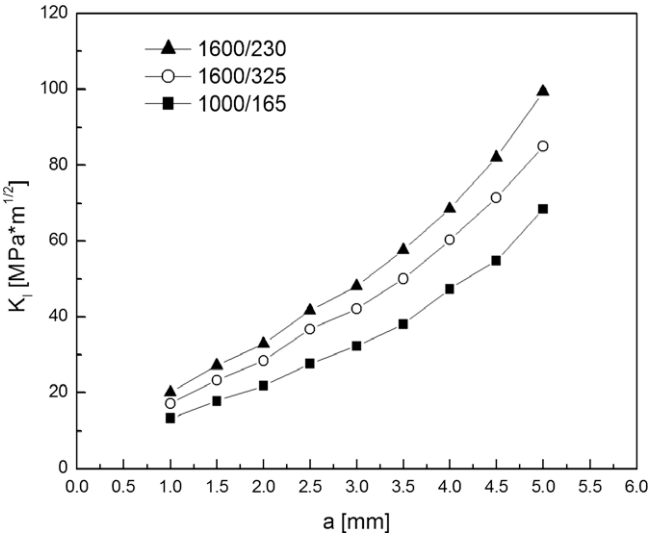

Fig. 12. K_I as a function of crack length for the different studied welds.

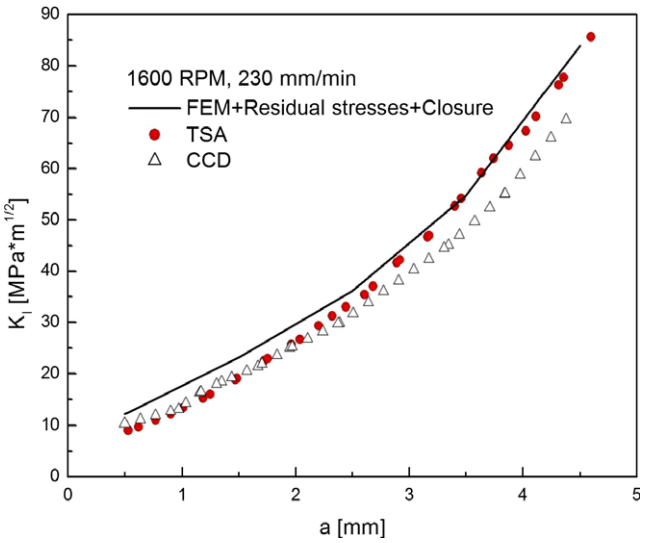

Fig. 13. K_I as a function of crack length for the specimen welded at 1600 RPM, 230 mm/min calculated with FEM and measured with TSA and CCD observations.

increasing the cyclic loading reveals that the stress concentration zone increases also with stress.

The results of ABAQUS simulations were used to calculate the theoretical K_I values at different crack lengths. In Fig. 11 it is shown the Von Mises stress distribution around the crack tip for the specimen welded at 1600 RPM and 230 mm/min and the corresponding stress field map for a crack length of 2 mm. From FEM calculations, the SIF values as a function of the crack lengths were obtained with simple extrapolation methods and plotted in Fig. 12. In such calculations it was not considered the residual stresses effects and consequently the effective values of the stress intensity factors. To take into account such residual stresses effects it was calculated their contribution to the K_I value as follow:

$$K_I = \int_0^a S_0(x) m(x,a) \mathrm{d}x \tag{2}$$

where S_0 is the residual stresses profile along the crack path, $m(x,a)$ is a weight function and m_1 and m_2 its coefficients:

$$m(x,a) = \frac{\left[1 + m_1\left(1 - \frac{x}{a}\right) + m_2\left(1 - \frac{x}{a}\right)^2\right]}{\sqrt{2\pi(a-x)}}$$
$$m_1 = 0.61 + 17.19\left(\frac{a}{W}\right)^2 + 8.79\left(\frac{a}{W}\right)^6 \tag{3}$$
$$m_2 = 0.25 + 3.29\left(\frac{a}{W}\right)^2 + 70.04\left(\frac{a}{W}\right)^6$$

The contribution due to crack closure effect was instead estimated by the following equation:

$$K_{\text{aperture}} = C\sigma_{\text{aperture}}^{\sqrt{\pi a}}$$
$$C = 1.12 - 0.231\left(\frac{a}{W}\right) + 10.55\left(\frac{a}{W}\right)^2 - 21.72\left(\frac{a}{W}\right)^3 + 30.39\left(\frac{a}{W}\right)^4 \tag{4}$$

The corrected K_I behaviour as a function of the crack length compared with those belonging to the calculations performed with CCD camera observations and TSA is plotted in Fig. 13. As a general behaviour, the experimental curves tend to underestimate the K_I value at fixed crack length; after few mm of crack propagation the TSA measurements are coincident with the theoretical model while the CCD camera calculations continue to underestimate the SIF. Interesting conclusion is that both the experimental methods well agree with good approximation with themselves, while also the theoretical values are in good agreement, giving rise to error difference well below 10%. An idea of the crack evolution, in different moments of cyclic loading, can be obtained by the observation of the crack path in Fig. 14.

4. Conclusions

The room temperature fatigue and crack behaviour properties of AA6082 friction stir welded joints were studied and the results

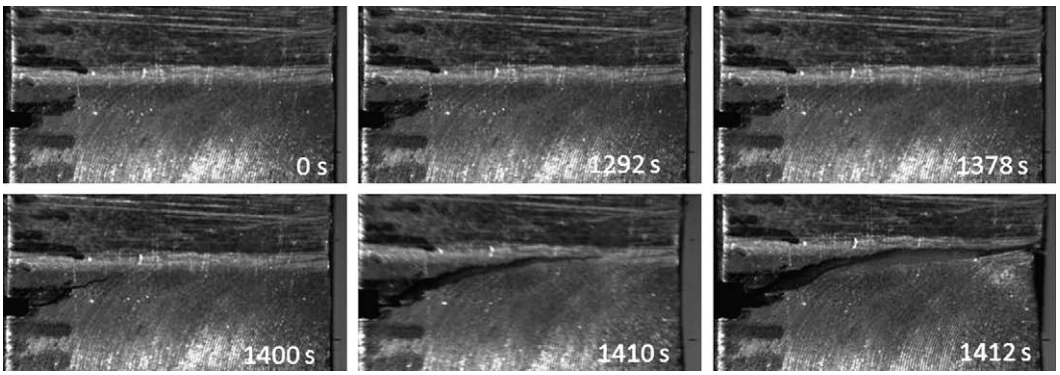

Fig. 14. Crack path in the FSW joints during cyclic loading.

were presented in the present paper. The employed rotating speeds and advancing speeds of the threaded tool were 1600 RPM, 230, 325, 460 mm/min and 1000 RPM, 165, 230 and 325 mm/min, respectively. The joints welded with a rotation speed of the tool of 1600 RPM and a travel speed of 230 mm/min showed the highest fatigue resistance, the samples welded at 1600 RPM 325 mm/min and 1000 RPM 165 mm/min experienced a very similar behaviour at high stress amplitude. The fatigue crack rate as a function of ΔK for all the joints showed that the joints welded with a rotating speed of 1000 RPM are more sensitive to crack initiation respect to the ones obtained at 1600 RPM. In addition the joints welded at 1600 RPM show a crack growth rate lower than those welded with a rotating speed of 1000 RPM. All the fatigue crack tests were monitored via thermoelastic stress analysis and CCD camera observations, as a general behaviour the experimental curves tend to underestimate the K_I value at the same crack length, after few mm of crack propagation the TSA measurements are coincident with the theoretical model while the CCD camera calculations continue to underestimate the SIF.

References

[1] Mishra RS, Ma ZY. Friction stir welding and processing. Mater Sci Eng R 2005;50:1–78.
[2] Guerra M, Schmidt C, McClure JC, Murr LE, Nunes AC. Flow patterns during friction stirwelding. Mater Charac 2003;49:95–101.
[3] Ulysse P. Three-dimensional modeling of the friction stir-welding process. Int J Mach T Manuf 2002;42:1549–57.
[4] Cavaliere P, Squillace A, Campanile G, Panella F. Effect of welding parameters on mechanical and microstructural properties of AA6056 joints produced by friction stir welding. J Mater Proc Tech 2006;180:263–70.
[5] Hatamleh O, Lyons J, Forman R. Laser and shot peening effects on fatigue crack growth in friction stir welded 7075–T7351 aluminum alloy joints. Int J Fatigue 2007;29:421–34.
[6] John R, Jata KV, Sadananda K. Residual stress effects on near-threshold fatigue crack growth in friction stir welds in aerospace alloys. Int J Fatigue 2003;25:939–48.
[7] Dickerson TL, Przydatek J. Fatigue of friction stir welds in aluminium alloys that contain root flaws. Int J Fatigue 2003;25:1399–409.
[8] James MN, Bradley R, Lombard H, Hattingh DG. The relationship between process mechanisms and crack paths in friction stir welded 5083-H321 and 5383-H321 aluminium alloys. Fatigue Fract Eng Mater Struct 2005;28:245–56.
[9] Ericsson M, Sandstrom R. Influence of welding speed on the fatigue of friction stir welds, and comparison with MIG and TIG. Int J Fatigue 2003;25:1379–87.
[10] Cavaliere P, Nobile R, Panella FW, Squillace A. Mechanical and microstructural behaviour of 2024-7075 aluminium alloy sheets joined by friction stir welding. Int J Mach T Manuf 2006;46:588–94;
Hori H, Makita S, Hino H. Friction stir welding of rolling stock for subway. Proceedings of the first international symposium on friction stir welding, Thousand Oaks, CA, USA; June 14–16, 1999.
[11] Cavaliere P, Squillace A. Effect of welding parameters on mechanical and microstructural properties of dissimilar AA6082-AA2024 joints produced by friction stir welding. Mater Sci Forum 2006;519–521:1163–8.
[12] Chan RW, editor. Concise encyclopedia of materials characterization. Elsevier Science Publishers; 2005. p. 707.
[13] Luong MP. Thermography: a new nondestructive evaluation method in fatigue damage. Mech Mater 1998;28:155–63.
[14] Hermanson KS, Sandor BI. Corrosion fatigue modeling via differential infrared thermography. Ex Tech 1998;22:19–21.
[15] Yang B, Liaw PK, Wang H, Huang JY, Kuo RC, Huang JG. Thermography: a new nondestructive evaluation method in fatigue damage. JOM-e 2003:55.
[16] Zhang D, Sandor BI. ASTM STP 1991;1122:341–53.
[17] Tomlison RA, Olden EJ. Thermoelasticity for the analysis of crack tip stress fields-a review. Strain 1999;35:49–55.
[18] Dìaz FA, Patterson EA, Tomlison RA, Yates JR. Measuring stress intensity factors during fatigue crack growth using thermoelasticity. Fatigue Fract Eng Mater Struct 2004;27:571–83.
[19] Harwood N, Cummings WM. Thermoelastic stress analysis. Adam Hilger 1991.
[20] Belgen MH. Structural stress measurements with an infrared radiometer. ISA Trans 1967;6:164–77.
[21] Cavaliere P, Rossi GL, Di Sante R, Moretti M. Thermoelasticity for the evaluation of fatigue behavior of 7005/Al2O3/10p metal matrix composite sheets joined by FSW. Int J Fatigue 2008;30:198–206.
[22] Huang YM, Abdel Mohsen HH, Rowlands RE. Determination of individual stresses thermoelastically. Ex Mech 1990;30:88–94.
[23] Lesniak JR. Thermoelastic data improvements. Proceedings of SEM Spring Conference on Experimental Mechanics, Dearborn Michigan 1993:721–9.
[24] Offermann S, Beaudoin JL, Bissieux C, Frick H. Thermoelastic stress analysis under nonadiabatic conditions. Ex Mech 1997;37:409–13.
[25] John R, Jata KV, Sadananda K. Residual stress effects on near-threshold fatigue crack growth in friction stir welds in aerospace alloys. Int J Fatigue 2003;25:939–48.
[26] Cavaliere P. Crack tip plasticity in plastically graded Ni–W electrodeposited nanocrystalline alloys. Comput Mater Sci 2008;41:440–9.